Measurement of electron-impact excitation into the $3p^5 3d$ and $3p^5 5s$ levels of argon using Fourier-transform spectroscopy

J. Ethan Chilton and Chun C. Lin
Department of Physics, University of Wisconsin, Madison, Wisconsin 53706
(Received 13 May 1999)

Cross sections for direct electron-impact excitation from the ground level into the $3p^5 5s$ and $3p^5 3d$ levels are measured for incident electron energies from threshold to 200 eV. The optical cross sections for the $3p^5 5s \rightarrow 3p^5 4p$ and $3p^5 3d \rightarrow 3p^5 4p$ emissions yield the apparent excitation cross sections. The cascade cross sections are obtained by measuring the emission intensities for transitions into $3p^5 5s$ and $3p^5 3d$ from the higher levels, and are subtracted from the apparent excitation cross sections to give the direct excitation cross sections. Most of the emission lines are in the infrared region, requiring the use of Fourier-transform spectroscopic techniques. The general trends of the cross-section results are discussed. Excitation cross sections for the $3p^5 4f$ levels are also reported. Because our experiments do not extend to the vacuum ultraviolet, the direct excitation cross sections for the levels optically connected to the ground state were not obtained.
[S1050-2947(99)03911-6]

PACS number(s): 34.80.Dp, 34.80.My

I. INTRODUCTION

Electron-impact excitation of argon is a process of interest in the fields of lasers, plasma processing, and lighting technology. Cross sections for the various excitation channels are needed for accurate modeling of plasmas and for plasma diagnostic measurements. These cross sections are generally determined using the optical method, wherein the intensity of emissions from excited atoms is measured at a known atomic density and incident beam flux using photomultiplier tubes (PMT). For rare-gas atoms such as argon, many of the low-lying excited levels emit infrared (IR) radiation, which is difficult to detect using conventional dispersive spectroscopic techniques. Semiconductor detectors, which operate in the IR regions, have low detectivity and signal-to-noise ratios that make them unfeasible to use with monochromators. The large number of narrowly spaced emission lines also makes the use of narrow-band optical filters impractical. Previous work in our lab [1–3] has demonstrated the utility of the Fourier-transform spectrometer (FTS) in weak emission IR experiments such as these. The FTS combines a large throughput with the ability to simultaneously acquire data on all lines within a large spectral region, allowing us to investigate IR atomic transitions.

Figure 1 shows an argon energy level diagram. The first excited configuration, $3p^5 4s$, has been previously studied [4,5]. Emissions out of the next configuration, $3p^5 4p$, produced by electron impact, lie in the visible spectral region and have been extensively studied [6,7]. However, the $3p^5 3d \rightarrow 3p^5 4p$ and $3p^5 5s \rightarrow 3p^5 4p$ transitions, which are important contributors to the $3p^5 4p$ population through radiative decay, are all infrared. In a previous paper [1] we described the use of the FTS technique to measure these transitions. By subtracting these IR contributions to the $3p^5 4p$ population from the total population provided by the observed $3p^5 4p \rightarrow 3p^5 4s$ excitation cross sections, the cross sections for direct electron-impact excitation into the $3p^5 4p$ levels were determined and reported in Ref. [1].

Studies of the cascades into the $3p^5 4p$ levels have also resolved the puzzle of certain unusual pressure effects in the excitation of rare gases. It has been known that the measured optical (and apparent) cross sections for the $3p^5 4p \rightarrow 3p^5 4s$ emission lines vary significantly with the gas pressure, even at pressures as low as 1 mTorr. (For the corresponding emission cross sections of Xe, this pressure dependence sets in at 0.1 mTorr.) The $3p^5 4p$ levels are not optically connected to the ground state. At first sight, we do not expect the kind of pressure dependence associated with excitation into optically allowed levels arising from radiation trapping. Another cause of the pressure dependence is collisional excitation transfer, but its effects are expected to be minimal at these low pressures. This anomaly was resolved by the measurements of the cascade cross sections for the various transitions into the $3p^5 4p$ levels. The total cascade cross sections are found to have the same pressure dependence as the apparent cross sections, so that when the former is subtracted from the latter, the resulting direct excitation cross sections are independent of the pressure [1]. Excitation

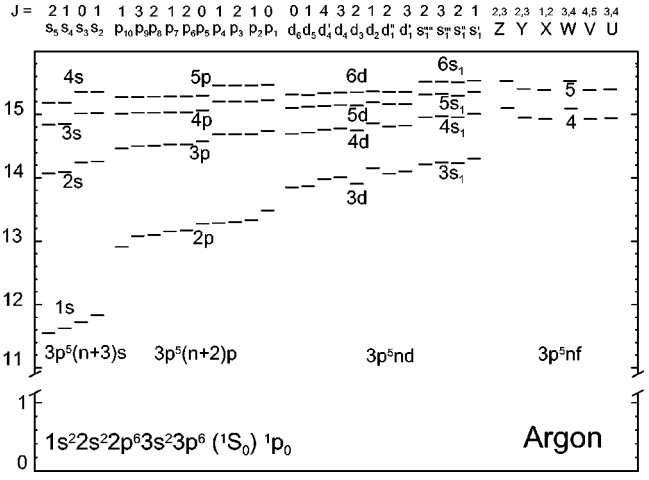

FIG. 1. Argon energy-level diagram in units of eV. Configuration notation for the excited manifolds is listed at the bottom. We refer to individual levels within a manifold with Paschen's notation.

 ©1999 The American Physical Society

cross sections for the optically allowed levels ($3p^5ns$ and $3p^5nd$ with $J=1$) have an intrinsic pressure dependence due to radiation trapping. This pressure dependence propagates to other levels through successive cascades. For an optically nonallowed level, the pressure dependence of the apparent excitation cross sections is entirely from cascade. To determine the direct excitation cross sections, the choice of pressure is not critical so long as both the apparent and cascade cross sections were measured at the same pressure. Similar measurements of the cascade radiation into the $5p^56p$ levels of Xe have been made [2]. With the proper cascade subtraction, the direct excitation cross sections for the Xe($5p^56p$) levels are shown to be independent of the pressure, in spite of the extraordinarily strong pressure dependence of the apparent cross sections [2].

In this paper, we study electron-impact excitation of the $3p^53d$ and $3p^55s$ levels. Measurements of the infrared $3p^53d \rightarrow 3p^54p$ and $3p^55s \rightarrow 3p^54p$ emissions furnish the total population of the $3p^53d$ and $3p^55s$ levels. However, to determine their direct electron-impact excitation cross sections, one must correct for the population due to radiative cascade. The latter is found by measuring the emission intensities of the transitions into $3p^53d$ and $3p^55s$ from the higher levels. These transitions have wavelengths as high as 6 μm, at which the detectors are much less sensitive compared to the region around 1.6 μm. Lock-in detection is incorporated into our FTS system to improve the sensitivity. The cross sections for the $3p^53d$ and $3p^55s$ levels so obtained, along with results of the $3p^54s$ and $3p^54p$ reported earlier, constitute a comprehensive set of excitation cross sections needed for a basic quantitative understanding of the electron-atom processes, and a data basis for technological applications in such areas as plasmas, discharges, and lighting.

A caveat concerning our particular experiments should be made. The $J=1$ levels in the $3p^53d$ and $3p^55s$ configurations are optically coupled to the ground state and emit in the deep ultraviolet (UV) at 86–89 nm. Because our apparatus is not designed to operate below 220 nm, we could not acquire data on the $3p^55s$ and $3p^53d$ resonance lines. As we discussed in our previous paper [1], these lines experience reabsorption of emitted photons. The effective branching fractions for the unmeasured $3p^55s$ and $3p^53d$ resonance emissions are pressure-dependent and cannot be determined by using just the oscillator strengths of the emission lines from the resonance levels. We therefore do not report cross sections for these levels. We do provide apparent excitation functions for these levels and discuss their general features in Sec. IV.

II. OPTICAL METHOD

We employ the optical method to determine electron-impact excitation cross sections. This method has been more extensively reviewed elsewhere [8], and will be discussed here only briefly.

Consider an electron beam of current I traversing a gas of number density n_0. Some of the atoms will be excited to level a, and then decay to lower level b, emitting a photon. If we measure the number of photons emitted per unit time per unit beam length, Φ_{ab}, then we may define an *optical emission cross section* for the $a \rightarrow b$ transition:

$$Q_{ab}^{\mathrm{opt}} = \frac{\Phi_{ab}}{(I/e)n_0}, \tag{1}$$

where e is the electronic charge. The sum of all optical cross sections for emission out of a level into all the lower levels is termed the *apparent cross section*, and the sum of all optical cross sections for emission into a level out of all the higher levels is termed the *cascade cross section*:

$$Q_a^{\mathrm{app}} = \sum_{b<a} Q_{ab}^{\mathrm{opt}}, \quad Q_a^{\mathrm{casc}} = \sum_{c>a} Q_{ca}^{\mathrm{opt}}. \tag{2}$$

The direct electron excitation cross section is then equal to the difference between the apparent and cascade cross sections:

$$Q_a^{\mathrm{dir}} = Q_a^{\mathrm{app}} - Q_a^{\mathrm{casc}}. \tag{3}$$

To obtain the apparent excitation cross sections, the $3p^55s \rightarrow 3p^54p$ (0.9–1.4 μm) and $3p^53d \rightarrow 3p^54p$ (0.9–1.5 μm) transitions are used. For cascades into the $3p^55s$ levels, transitions from the $3p^55p$, $3p^56p$, and $3p^57p$ configurations (2–6 μm, 1.1–1.6 μm, and 0.9–1.2 μm respectively) are within the range of our FTS, whereas transitions from the higher configurations can be studied using our PMT/monochromator system [1,8]. Similarly, combination of the FTS and the PMT/monochromator system covers all the cascade radiation into the $3p^53d$ levels.

III. EXPERIMENTAL APPARATUS

A. Collision chamber

The argon atoms studied in the experiments comprise a static gas target contained in a stainless-steel collision chamber. A diffusion pump (700 liters/s) evacuates the chamber to a base pressure of 10^{-8} Torr. An ion pump is used to maintain vacuum when the experiment is not in use. During data acquisition, the vacuum pumps are valved off and the chamber filled with research grade argon to the desired pressure. A getter pump eliminates any remaining contaminants. The pressure is recorded with a capacitive manometer. Figure 2 shows the layout of the experiment.

The electron gun is attached to one of the collision chamber's ConFlat end flanges. It consists of an indirectly heated BaO cathode, with multiple electrostatic focusing and acceleration grids, producing an electron current between 200 and 500 μA over energies of 10 to 250 eV. The beam is approximately 3 mm in diameter with an energy resolution of about 0.6 eV (full width at half maximum). A deep Faraday cup collects the electrons, and the current is recorded by a digital multimeter. A control grid is placed directly in front of the cathode. By supplying a large 1 kHz square wave to this grid, the electrons can be deflected from the gun, modulating the electron beam so that a lock-in detector may be employed. Detecting this modulated signal also allows us to remove the signal due to scattered photons from the hot cathode.

A slit in the Faraday cup allows the radiation to emerge and pass through a CaF_2 window on the side of the chamber.

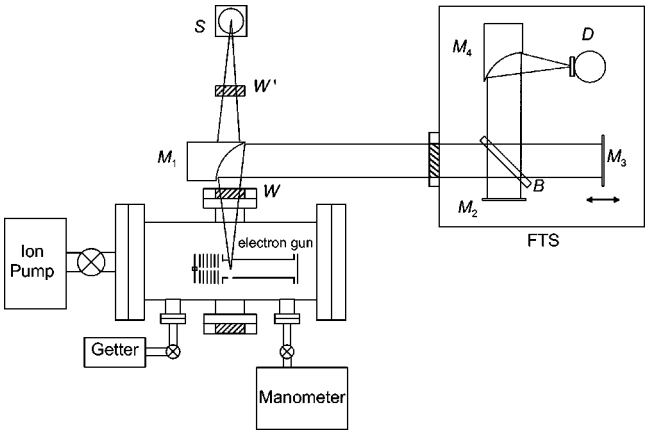

FIG. 2. Experimental layout. Radiation from excited atoms emerges from the chamber through the window, *W*, and is reflected off mirror M_1 into the FTS. The light passes through the beamsplitter (*B*) and is reflected off the fixed and moving mirrors, M_2 and M_3. The interference pattern is focused by mirror M_4 onto the detector, *D*. Mirror M_1 can be rotated to observe the output of a calibrated blackbody source (*S*), through a compensating window W'.

An off-axis parabolic mirror collects the light and sends a collimated beam into the FTS.

B. FTS and detection electronics

A FTS is a Michelson interferometer, consisting of a fixed and moving mirror and a self-compensating beamsplitter [9]. Light entering the spectrometer is split into two beams, which are reflected by the two mirrors, then recombined at a detector. The signal intensity is recorded as a function of displacement of the moving mirror, resulting in an interferogram that can be Fourier transformed to yield a spectrum. The displacement of the moving mirror is detected by a 633 nm (15 798 cm^{-1}) He-Ne laser, following the same optical path, and a laser photodetector, which detects the fringes of the laser interference pattern. The number of data points collected to produce the interferogram depends on the wavelength range of the detector. If the detector is sensitive to radiation between 15 798 and 7899 cm^{-1}, two data points must be collected per laser cycle (once per each minimum at the laser detector), to prevent aliasing of radiation from shorter to longer wavelengths of the spectrum, according to the Nyquist criterion [9]. Below 7899 cm^{-1}, it is sufficient to collect one point per laser cycle.

The FTS used in this experiment is a Nicolet Magna-860 spectrometer. KBr windows allow the infrared radiation from the chamber to enter the device. Two different beamsplitters were used in the experiment. A quartz beamsplitter was used for near-IR work, and a KBr beamsplitter for longer wavelengths. Three detectors were employed. A thermoelectrically cooled $In_xGa_{1-x}As$ detector covered the 0.9–1.6 μm region, with the quartz beamsplitter. A liquid-nitrogen-cooled InSb detector was used for 1.3–2.7 μm, with the KBr beamsplitter, and a second longer-wavelength InSb detector for the 2.6–6 μm range. The signal from the detectors is fed to a digital lock-in amplifier, tuned to the 1 kHz modulation frequency of the electron beam.

The FTS was run in step-scan mode. For a spectral resolution of 2 cm^{-1}, the moving mirror needs to travel a total displacement of 5 mm. For the $In_xGa_{1-x}As$ detector, with a spectral range of 12 000–5900 cm^{-1}, two data points need to be taken per laser cycle, for a total of 15 798 position points of the moving mirror to generate an interferogram. The mirror is moved until the laser photodetector senses a null in the interference pattern, and is then stopped. After resting for five times the lock-in amplifier's time constant, the demodulated signal from the lock-in at that mirror position is recorded as the interferogram data point. The mirror is then stepped to the next position. For the $In_xGa_{1-x}As$ detector with a 10 ms lock-in time constant and 50 ms of data recorded at each position, the data collection time was approximately half an hour per interferogram. For the InSb detectors, which do not see above 7899 cm^{-1}, only one data point need be recorded per laser cycle. However, these detectors have a lower detectivity than the $In_xGa_{1-x}As$, so a time constant of 100 ms, with 200 ms of data collected per position, was used, for a total data collection time of approximately 1.5 h per interferogram.

Once the interferogram is recorded, the FTS software computes the Fourier transform, using Happ-Genzel apodization and power spectrum phase correction. The result is an unnormalized spectrum of peaks corresponding to the various atomic transitions.

C. Calibration

To transform between the peak heights recorded by the FTS and normalized cross sections, two separate calibrations must be performed. First, the heights of the peaks must be adjusted to allow for the transmission of the various optical elements and the quantum efficiency of the detector. To do this, the parabolic mirror M_1 (in Fig. 2) is rotated 180° and the output of a calibrated blackbody source (*S*) is sent into the FTS. A CaF_2 window, identical to that on the collision chamber, is placed in the beam path for compensation. The spectrum recorded by the FTS is then divided by the theoretical blackbody curve. The result is an instrument response function for the particular detector/beamsplitter combination. Now, each electron excitation spectrum can be divided by this response function to yield a corrected spectrum in which the height of each peak is proportional to the number of photons emitted in the particular transition.

Dividing the peak heights by the electron beam current and pressure yields a number proportional to the cross sections, as defined in Eq. (1). To place these relative numbers on an absolute scale, we must perform a bridging calibration. Our previous paper [1] detailed the use of a monochromator/PMT system to determine the absolute cross section of the $2p_{10} \rightarrow 1s_5$ (Paschen's notation) transition in argon. This line lies at 912.3 nm, and is visible in both a PMT (S-1 photocathode) and the $In_xGa_{1-x}As$ detector. All lines in the $In_xGa_{1-x}As$ region can now be ratioed to the 912.3 nm line and thus be placed on an absolute scale. The spectrum of lines observed in the InSb detector can likewise be absolutely calibrated by ratioing them to lines in the overlap region (1.3–1.6 μm) between the InSb and $In_xGa_{1-x}As$ detectors.

In connection to the radiometric calibration, it is necessary to check the anisotropy of the radiation. For this purpose we placed a polarizing filter into the beam path in order to determine the amount of polarization of the emission lines. The electron excitation signal was examined with the polarizer oriented in both the parallel and perpendicular positions. The ratio of these signals was compared to the response of the detector to an unpolarized broadband source with the polarizing filter in the same orientations. We find the polarization factor P of emissions from the $3p^5 4p$, $3p^5 5s$, and $3p^5 3d$ levels to be too small (generally less than 16%), across all energies studied. Since the polarization correction introduces only a factor of $(1-P/3)$ to the cross sections, the anisotropy of the radiation amounts to no more than a 5% correction [8], which is less than the statistical uncertainty of our measurements.

D. Data acquisition

Data were acquired at an argon pressure of 6 mTorr. Excitation functions were collected between onset and 200 eV by recording several spectra using the method described in Sec. III B. Peak heights were then extracted and averaged for each transition, and divided by the electron beam current and pressure. The results were calibrated as described above.

Some transitions with wavelengths within our spectral detection range were not observed, owing to their small cross sections. By observing the amplitude of noise recorded in that spectral region, it is possible to place an upper bound on the size of the transition. These upper bounds formed negligible contributions to the total cascade cross sections.

The spectral region studied in this experiment includes the 1.4 μm and 4.3 μm CO_2 and 1.9 μm and 2.7 μm H_2O molecular absorption bands. Radiation emitted from the collision chamber passes through approximately one meter of air before entering the spectrometer. Absorption of the input radiation by CO_2 and H_2O is accounted for by the blackbody calibration procedure described in Sec. III C. To ensure proper calibration of the few lines in the CO_2 and H_2O absorption region, the relative humidity and temperature in the lab were monitored, and the calibration procedure repeated in the case of variations. The relative uncertainties of these lines have been adjusted accordingly.

In our previous work [1], we demonstrated the importance of resonance radiation reabsorption as a population mechanism for the excited states of argon. Increasing argon pressure tends to increase the optical cross sections, as defined by Eq. (1). Hence, it is vital to realize that the *apparent* cross sections quoted in this paper are correct only for the pressure at which data were acquired (6 mTorr), and may vary with pressure. As explained in Sec. I, both the apparent and cascade cross sections must be measured at the same pressure, and the resulting *direct* electron-impact excitation cross sections are independent of pressure. We choose our pressure at 6 mTorr so as to optimize the emission signal at wavelengths above 2 μm (because of the low sensitivity of InSb), while keeping the pressure low enough to maintain proper focusing of the electron beam.

At each pressure and energy studied, several step-scan runs were taken. The extracted peak heights for each transition were then averaged, providing statistical error bars for each data point. The absolute calibration procedure [1] is estimated to have a systematic uncertainty of around 12%. The systematic uncertainty in the FTS data, due to the calibration procedure, pressure, and current measurement, is estimated to be 15%. For each measurement, we quote a combined statistical and systematic uncertainty. Because the direct cross sections are calculated as the difference between two other measurements [Eq. (3)], it is possible that small percentage error bars on the apparent and cascade cross sections can produce relatively large percentage error bars on the direct cross sections, particularly if the cascade and apparent are close in magnitude.

IV. RESULTS AND DISCUSSION

Interpretation of the electron-impact excitation cross-section data of the heavier rare gases is facilitated by utilizing the well-established results of helium with modifications to account for deviations from the L-S coupling. Furthermore, each excited configuration of the type $n'p^5 nl$ contains numerous levels, and the cross sections of these levels are related to their J values in a fundamental way. In this section, we first summarize the general principles derived from basic theoretical considerations. Our experimental results are then presented and analyzed based on these principles.

A. General principles

1. Shape of the excitation functions

In the case of helium, excitation from the ground level 1^1S to the optically allowed levels n^1P is characterized by large cross sections and a broad peak in the excitation function (cross section versus incident electron energy). For the singlet levels not optically connected to the ground level, such as n^1S and n^1D, the cross sections are smaller and the excitation functions are less broad in comparison with the n^1P levels. Most striking is the case of spin-changing excitation, i.e., from 1^1S to n^3L, in which the excitation functions exhibit a sharp peak near the energy threshold [10].

For the heavier rare-gas atoms, the ground state $1s^2 2s^2 \cdots n'p^6$ is a $^1S_0$ level, but most of the excited states do not conform to the L-S coupling, so that the designation of spin-multiplicity is not always valid. Nevertheless, one can always express the excited-state wave functions as linear combinations of the L-S eigenfunctions, which one can correlate with the rules in the preceding paragraph. For instance, the Ar($3p^5 3d$) configuration yields the following L-S terms: $^1P_1$, $^3P_0$, $^3P_1$, $^3P_2$, $^1D_2$, $^3D_1$, $^3D_2$, $^3D_3$, $^1F_3$, $^3F_2$, $^3F_3$, and $^3F_4$. To allow for deviation from the L-S coupling, one regards each level in this configuration as a superposition of the L-S terms. Since J is always a good quantum number, such mixing is limited to L-S terms of the same J. Thus, the $J=0$ and $J=4$ levels of the $3p^5 3d$ configuration are purely triplet states ($^3P_0$ and $^3F_4$, respectively) and their excitation functions are expected to be sharply peaked near the threshold. The $3p^5 3d$ configuration contains also three levels with $J=3$ (superpositions of $^1F_3$, $^3F_3$, and $^3D_3$), four levels with $J=2$ (superpositions of $^1D_2$, $^3D_2$, $^3P_2$, and $^3F_2$), and three levels with $J=1$ (superpositions of $^1P_1$, $^3P_1$, and $^3D_1$). Since these ten levels all contain a singlet component in the L-S superposition, excitations from the

ground level ($^1S_0$) into the $J=3$, $J=2$, and $J=1$ levels generally show broader excitation functions compared to excitation into the $J=0$ and $J=4$ levels, which have no singlet components. Moreover, the $J=1$ levels contain the $^1P_1$ term, which is optically connected to the ground level. Thus the excitation functions of the $J=1$ levels should, in general, have the broadest peaks. Exceptions to the above rules occur if the singlet component of a particular level is very small, as will be discussed in Sec. IV B.

2. Magnitudes of the cross sections

A simple, useful picture to describe the qualitative features of excitation cross sections is to regard the excitation process as an absorptionlike transition induced by the electromagnetic field associated with the incident electron. This field can be decomposed into the monopole ($k=0$), dipole ($k=1$), quadrupole ($k=2$), etc. components. Excitation from the ground state of helium into the n^1S, n^1P, and n^1D levels can be associated with the monopole, dipole, and quadrupole fields, respectively. This multipole field picture addresses the effect of Coulomb interaction in electron excitation, but does not allow for electron exchange. Consequently, it is not applicable to spin-changing excitations like $1^1S \rightarrow n^3L$. The multipole-field analysis has been successfully applied by Purcell [11] to calculate the hydrogen $2^2S \rightarrow 2^2P$ transition induced by collisions with electrons and ions.

Application of this multipole-field picture to argon has been made to discuss the cross sections for excitation into the $3p^5 4p$ levels from the metastable levels ($3p^5 4s$, $J=0$ and 2) and their relation to the cross sections from the ground level [12]. In this paper we further extend the multipole-field analysis to excitation from the ground level ($3p^6\ ^1S_0$) to the $3p^5 3d$ levels. Since we are dealing with a transition from $3p$ ($l=1$) into $3d$ ($l=2$), only the dipole ($k=1$) and octopole ($k=3$) components of the multipole field are operative. With the dipole field, it is possible to excite the ground level ($J=0$) into a level with $J=1$, whereas the octopole field leads to excitation into $J=3$ levels. Excitations from the ground state into the levels with $J=0,2,4$ do not satisfy the ''selection rules'' for $k=1$ and $k=3$ and must proceed through higher-order processes and/or electron exchange. Thus, at ''high'' energies, where the exchange effects are small, excitations from the ground state into the $3p^5 3d$ levels with odd J, in general, are favored over excitations into the even-J levels. Again, exceptions to the above rule may occur if any one of the $3p^5 3d$ levels with $J=1$ or $J=3$ has a very small singlet component, resulting in a reduction of the cross section below those of the even-J levels.

On the other hand, if we consider excitation into the $3p^5 4p$ configuration (in place of $3p^5 3d$), the $3p^6 \rightarrow 3p^5 4p$ ($3p$ to $4p$ transitions) entails only the monopole ($k=0$) and quadrupole ($k=2$) members of the multipole field. The monopole component leads to the $3p^6$, $J=0 \rightarrow 3p^5 4p$, $J=0$ excitation and the quadrupole component to $3p^6$, $J=0 \rightarrow 3p^5 4p$, $J=2$. In this case, we should find the even-J levels to have larger cross sections than the odd-J levels. This is indeed confirmed experimentally [1]. The reversal of the even/odd ordering from $3p^5 3d$ to $3p^5 4p$ is due to the opposite parity of the two configurations involved.

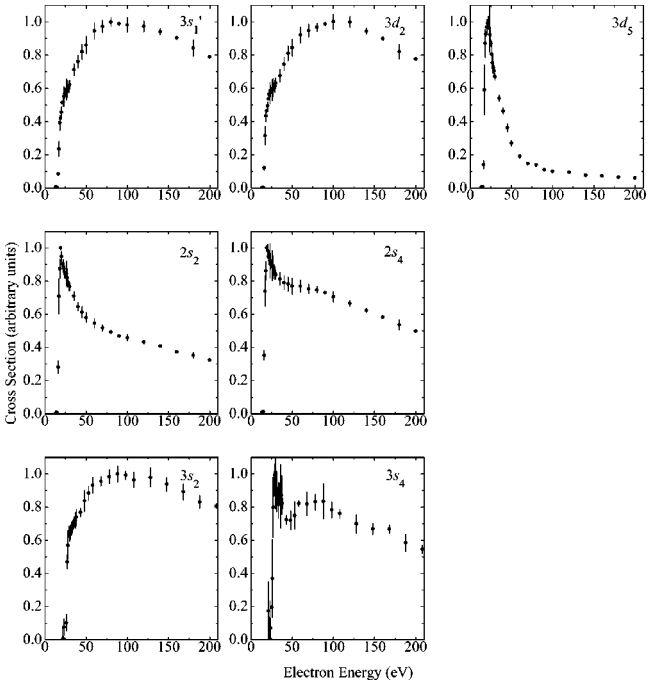

FIG. 3. Optical excitation functions for the three $J=1$ $3p^5 3d$ levels ($3s_1'$, $3d_2$, $3d_5$) and two $J=1$ $3p^5 5s$ levels ($2s_2$ and $2s_4$) studied. The two $J=1$ $3p^5 6s$ levels ($3s_2$ and $3s_4$) are shown for comparison. Each plot has been scaled to a maximum height of 1.0.

The multipole picture can be recast into a more formal, quantum-mechanical analysis [13]. Here we describe the n atomic electrons by $\vec{r}_j(r_j \theta_j \phi_j)$ and the incident electron by $\vec{r'}(r' \theta' \phi')$. The atom is excited from the initial state $\psi_i(J_i|\vec{r}_1, \ldots, \vec{r}_n)$ into the final state $\psi_f(J_f|\vec{r}_1, \ldots, \vec{r}_n)$ of total angular momenta J_i and J_f, respectively. Let us consider only the Coulomb interaction of the incident electron with the atom and neglect the exchange interaction. The collisional coupling potential between the initial and final atomic states, $C_{fi}(\vec{r'})$, is

$$C_{fi}(\vec{r'}) = \int \psi_f^*(J_f|\vec{r}_1, \ldots, \vec{r}_n) \times \left(\sum_j \frac{e^2}{|\vec{r'} - \vec{r}_j|} \right) \psi_i(J_i|\vec{r}_1, \ldots, \vec{r}_n) d\vec{r}_1 \ldots d\vec{r}_2 . \tag{4}$$

For our application, the initial state is $3p^6$ with $J_i=0$ and the final state is $3p^5 3d$ with J_f ranging from 0 to 3. Imagine that we construct ψ_i and ψ_f from the one-electron orbitals for the two configurations involved, and expand the Coulomb interaction by spherical harmonics as

$$\frac{1}{|\vec{r'} - \vec{r}_j|} = \frac{1}{r_>} \sum_{k,m} \frac{4\pi}{2k+1} \left(\frac{r_<}{r_>} \right)^k Y_{km}(\theta_j \phi_j) Y_{km}^*(\theta' \phi'), \tag{5}$$

where $r_<$ and $r_>$ are the lesser and greater of r' and r_j, respectively. Since the active electron moves from $3p$ into $3d$ ($l=1 \rightarrow l=2$), only the $k=1$ and $k=3$ terms in Eq. (5)

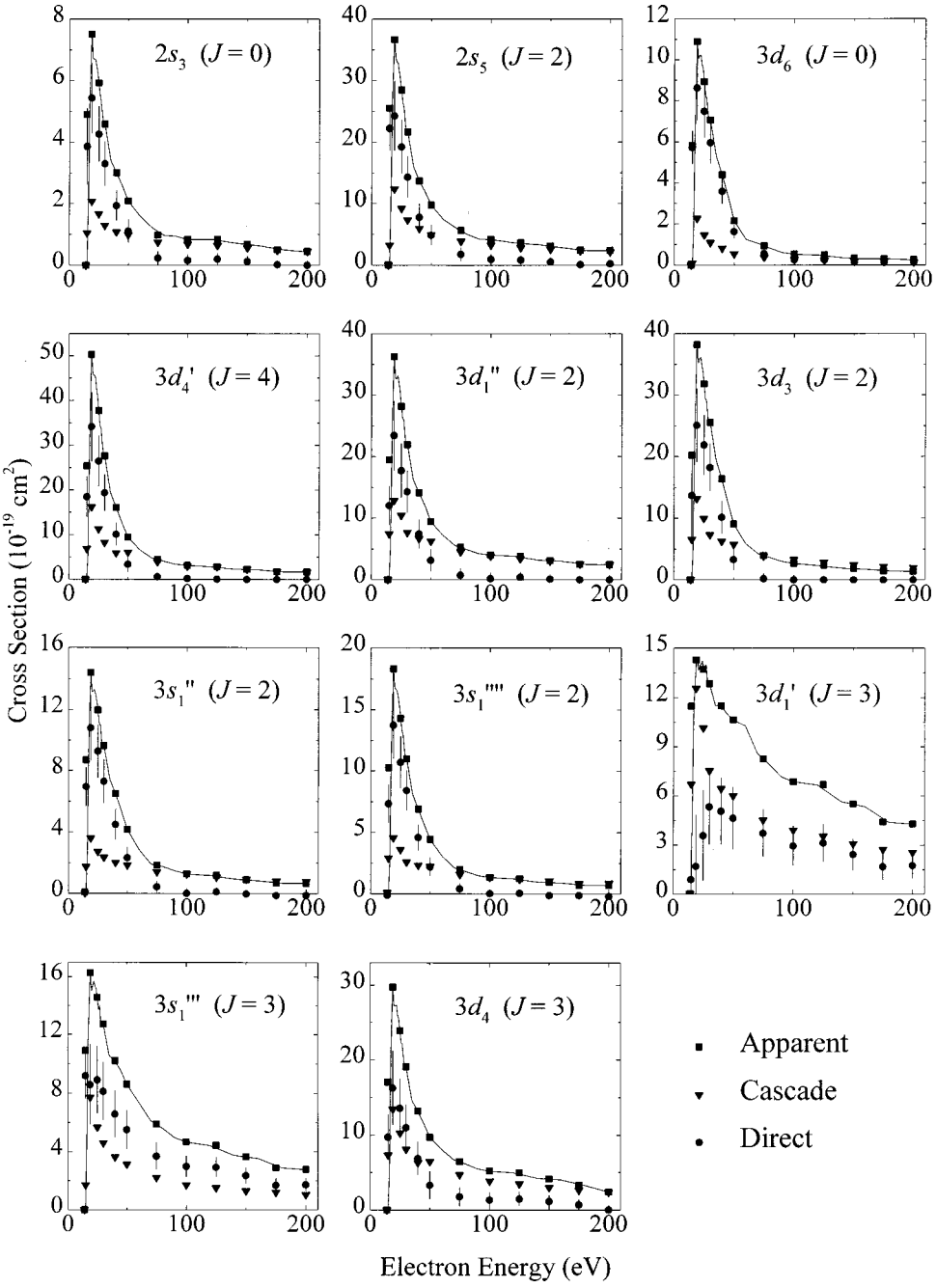

FIG. 4. Apparent, cascade, and direct excitation functions for the $3p^5 5s$ and $3p^5 3d$ levels. Error bars represent combined statistical and systematic uncertainties. The apparent and cascade cross sections are measured at a pressure of 6 mTorr. See the last paragraph of Sec. III D.

survive upon using Eq. (4) to integrate over the electron coordinates. This reduces the coupling potential C_{fi} into a mixture of integrals of triple products like $\psi_f^* Y_{k=1,m}(\theta_j \phi_j)\psi_i$ and $\psi_f^* Y_{k=3,m}(\theta_j \phi_j)\psi_i$. Since ψ_f, Y_{km}, and ψ_i are eigenfunctions of J corresponding to $J=J_f$, $J=k$, and $J=J_i=0$, respectively, all the above triple-product integrals, and therefore C_{fi}, vanish unless $J_f=1$ or $J_f=3$. To the first approximation, excitation cross sections are obtained from the corresponding coupling potential. Thus it is possible to excite the $J=1$ and $J=3$ levels via first-order Coulomb interaction, whereas excitation into the $J=0,2$, or 4 levels would require electron exchange interaction or a higher-order Coulomb process in which the initial and final states are coupled through intermediate states. At ''high'' incident electron energies where the exchange interaction contributes insignificantly to the excitation cross sections, excitation into the odd-J levels of the $3p^5 3d$ configuration generally should have larger cross sections than the even-J levels.

B. The $3p^5 3d$, $J=1$ levels

The apparent excitation functions for the three levels with $J=1$ of the $3p^5 3d$ configuration ($3s_1'$, $3d_2$, and $3d_5$) are shown in Fig. 3. For the $3s_1'$ and $3d_2$ levels, we indeed see a broad maximum near 80 eV characteristic of excitation into an optically allowed level. The $3d_5$ excitation function, however, exhibits a sharp peak near the threshold in contrast to what we expect for a $3p^5 3d$, $J=1$ level. To understand this anomaly, an intermediate-coupling calculation of the wave functions [14] for all the levels of the $3p^5 3d$ configuration has been performed [15]. The wave functions of the three J

TABLE I. Direct electron-impact excitation cross sections in units of 10^{-19} cm^2. The uncertainty is combined statistical and systematic.

	J	peak	30 eV	40 eV	50 eV	75 eV	100 eV
$2s_3$	0	5.4±1.1	3.3±0.7	1.9±0.5	1.1±0.4	0.23±0.23	0.15±0.15
$2s_5$	2	24±6	14±3	7.8±2.2	4.8±1.7	1.7±1.1	0.94±0.86
$3d_6$	0	8.6±1.6	6.0±1.0	3.6±0.6	1.6±0.3	0.56±0.15	0.26±0.10
$3d_1''$	2	23±6	14±3	7.4±2.4	3.2±1.8	$0.75^{+1.1}_{-0.75}$	$0.19^{+0.94}_{-0.19}$
$3d_3$	2	25±6	18±4	10±3	3.3±1.8	0.50±0.45	0.40±0.40
$3s_1''$	2	11±2	7.3±1.4	4.5±1.0	2.3±0.7	0.44±0.38	$0.05^{+0.28}_{-0.05}$
$3s_1'''$	2	14±3	8.4±1.6	4.6±1.1	2.2±0.8	0.42±0.41	0.18±0.18
$3d_1'$	3	5.3±2.3	5.3±2.3	5.1±2.0	4.6±1.9	3.7±1.5	3.0±1.2
$3d_4$	3	16±5	11±3	6.9±2.2	3.3±1.9	1.8±1.1	1.3±1.1
$3s_1'''$	3	9.2±2.2	8.1±2.0	6.6±1.6	5.5±1.3	3.7±0.9	3.0±0.7
$3d_4'$	4	34±8	19±4	10±3	3.4±1.8	$0.56^{+1.0}_{-0.56}$	$0.21^{+0.75}_{-0.21}$

$=1$ levels of $3p^5 3d$ are linear combinations of the $^1P_1$, $^3P_1$, $^3D_1$ eigenfunctions. The weightings of the $^1P_1$ component in the $3s_1'$, $3d_2$, and $3d_5$ wave functions are 57%, 42%, and 0.09%, respectively. This explains the sharp peak in the excitation function of the $3d_5$ level, as it is almost a purely triplet level because of the very small $^1P_1$ component.

We have measured the optical emission cross sections for all the $3p^5 3d \rightarrow 3p^5 4p$ emission lines. The three $J=1$ levels also decay into the ground level. These UV emissions are not measured in our experiments. Because of radiation trapping, the effective branching fractions of the unmeasured transitions at the pressure of our measurements are not known. This has prevented us from determining the apparent excitation cross sections (hence also the direct excitation cross sections) of the $3s_1'$, $3d_5$, and $3d_2$ levels.

C. The $3p^5 5s$, $J=1$ levels

The $3p^5 5s$ configuration contains four levels. The two $J=1$ levels ($2s_2$ and $2s_4$) are superpositions of the $^1P_1$ and $^3P_1$ L-S terms, whereas the other two are purely triplet levels, $^3P_0$ ($2s_3$) and $^3P_2$ ($2s_5$). The $2s_2$ and $2s_4$ levels are optically connected to the ground level ($1p_0$ in Paschen's notation), so that the effective branching fractions of the $2s_2 \rightarrow 1p_0$ and $2s_4 \rightarrow 1p_0$ channels are strongly influenced by radiation trapping. As with the case of the $3s_1'$ and $3d_2$ levels discussed in Sec. IV B, we are unable to obtain the apparent excitation cross sections of the $2s_2$ and $2s_4$ from our measured optical cross sections for the $3p^5 5s \rightarrow 3p^5 4p$ emission lines.

Our measurements of the optical cross sections for the $2s_2 \rightarrow 2p_3$ and $2s_4 \rightarrow 2p_8$ emissions yield the shape of the apparent excitation functions of the $2s_2$ and $2s_4$ levels, shown in Fig. 3. In both curves the peak immediately above the energy threshold appears to be in contradiction with the broad maximum near 80 eV that is expected of optically allowed levels. A close examination of the $2s_4$ curve, however, reveals a possible broad shoulder structure near 80 eV. The $2s_2$ and $2s_4$ levels receive cascade from the $3p^5 np$ levels, which have excitation functions peaking at about 20 eV. Thus, the peak at 20 eV in the $2s_4$ function may be the result of cascade superimposed on the direct excitation component, which has the usual broad maximum at 80 eV. The same applies also to the $2s_2$ level, since its apparent excitation function can be decomposed into a curve with a peak at 20 eV plus one with a broad maximum at 80 eV. For comparison, we include in Fig. 3 the apparent excitation functions for the $3s_2$ and $3s_4$ levels (the two $J=1$ levels from $3p^5 6s$). Here the broad maximum is the prominent feature. The sharp peak near the threshold is much reduced compared

TABLE II. Apparent, cascade, and direct cross sections at 40 eV and 6 mTorr in units of 10^{-19} cm^2. The final column lists the percent contribution of the $3p^5 nf$ transitions to the total cascade.

	J	Apparent	Cascade	Direct	nf Cascade
$2s_3$	0	3.0±0.9	1.1±0.3	1.9±0.9	
$2s_5$	2	14±4	5.9±2.0	7.8±2.2	
$3d_6$	0	4.4±1.5	0.81±0.24	3.6±0.6	0%
$3d_1''$	2	14±4	6.7±3.0	7.4±2.4	37%
$3d_3$	2	16±3	6.3±2.2	10±3	58%
$3s_1''$	2	6.5±1.9	2.0±1.6	4.5±1.0	13%
$3s_1'''$	2	6.9±1.8	2.3±0.9	4.6±1.1	48%
$3d_1'$	3	12±2	6.4±1.9	5.1±2.0	69%
$3d_4$	3	13±4	6.3±2.2	6.9±2.2	59%
$3s_1'''$	3	10±2	3.6±0.9	6.6±1.6	30%
$3d_4'$	4	16±5	5.9±2.4	10±3	84%

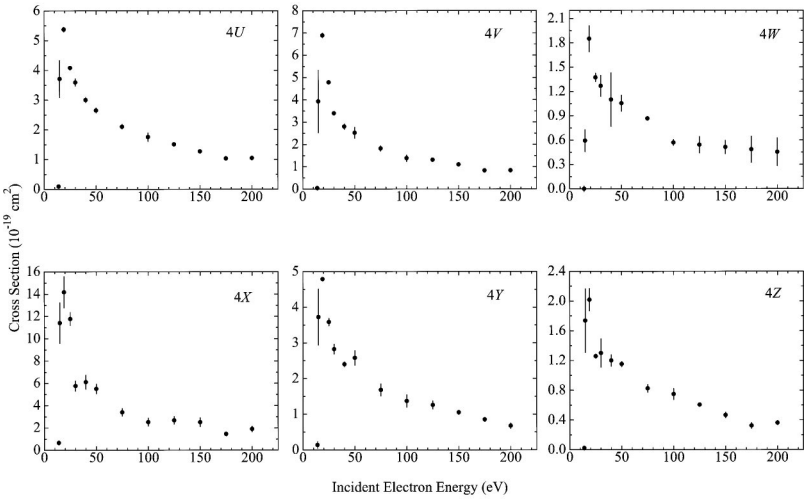

FIG. 5. Apparent excitation functions for the $3p^5 4f$ levels.

to the $2s_2$ and $2s_4$ levels, indicating a much smaller percentage contribution of cascade to the apparent excitation cross section.

D. $3p^5 3d$ and $3p^5 5s$ levels with $J \neq 1$

For all levels of the $3p^5 3d$ and $3p^5 5s$ configurations with $J \neq 1$, the only decay channels are the radiative transitions into the $3p^5 4p$ levels. From the optical emission cross sections of these transitions that we measured, the apparent excitation cross sections are obtained. We have also measured the optical emission cross sections for transitions into the $3p^5 3d$ and $3p^5 5s$ levels from the levels above them in order to determine the cascades. Most of the cascade into the $3p^5 5s$ levels is found to originate from the $3p^5 5p$ (2–6 μm), $3p^5 6p$ (1.1–1.6 μm), and $3p^5 7p$ (0.9–1.2 μm) configurations. For the $3p^5 3d$ levels, the cascade is predominantly due to the $3p^5 5p$ and $3p^5 6p$ levels (1.0–3.2 μm) as well as the $3p^5 4f$ (1.1–1.6 μm) and $3p^5 5f$ (0.9–1.1 μm) levels. The total cascade is then subtracted from the apparent excitation cross section to give the direct excitation cross section for each level.

Figure 4 summarizes the results of the apparent, cascade, and direct cross sections for the $J=0$ and $J=2$ levels of $3p^5 5s$ ($2s_3$ and $2s_5$), and the $J=0$ level ($3d_6$), the $J=4$ level ($3d_4'$), the $J=2$ levels ($3d_1''$, $3d_3$, $3s_1''$, $3s_1'''$), and $J=3$ levels ($3d_1'$, $3d_4$, $3s_1'''$) of $3p^5 3d$, over the energy range from threshold to 200 eV. Let us first focus on the shape of the direct excitation functions. The $2s_3$, $2s_5$, $3d_6$, and $3d_4'$ levels have purely triplet character. Excitation into these levels is entirely due to electron exchange and their excitation functions indeed have a sharp peak followed by a steep decline with increasing electron energy. More quantitatively, the excitation functions for these levels are expected to exhibit an E^{-3} dependence at high energies if one adopts the Ochkur approximation [16] to the Born theory. It should be interesting to see if our experimental data conform to this energy relation. For the four purely triplet levels, the direct excitation cross sections at high energies are small and were obtained as the difference between much larger quantities, i.e., the apparent and cascade cross sections. As a result, we have relatively large error bars on the direct excitation cross sections at high energies, as can be seen in Table I. Within the experimental uncertainties, energy dependences of E^{-n} with n ranging between 2.0 and 3.5 are all consistent with the high-energy cross sections for the purely triplet levels.

The $3d_1''$, $3d_3$, $3s_1''$, and $3s_1'''$ levels ($J=2$) have a partial singlet character ($^1D_2$), but they do not connect to the ground level through the $k=1$ and $k=3$ multipole ''selection rules'' (or these $J=2$ levels have no direct collisional coupling with the ground level via Coulomb interaction) as

TABLE III. Comparison of our cross-section results with those of Ref. [17]. Units are 10^{-19} cm^2.

	J	This work peak	Ref. [17] peak	This work 30 eV	Ref. [17] 30 eV	This work 50 eV	Ref. [17] 50 eV
$2s_3$	0	5.4±1.1	3.77	3.3±0.7	1.81	1.1±0.4	0.26
$2s_5$	2	24±6	22.2	14±3	10.8	4.8±1.7	1.52
$3d_6$	0	8.6±1.6	24.2	6.0±1.0	16.7	1.6±0.3	2.70
$3d_1''$	2	23±6	19.7	14±3	10.1	3.2±1.8	1.50
$3d_3$	2	25±6	99.3	18±4	65.2	3.3±1.8	10.7
$3s_1''$	2	11±2	14.4	7.3±1.4	7.68	2.3±0.7	1.08
$3s_1'''$	2	14±3	17.3	8.4±1.6	9.00	2.2±0.8	1.31
$3d_1'$	3	5.3±2.3	13.4	5.3±2.3	9.66	4.6±1.9	5.04
$3d_4$	3	16±5	31.6	11±3	19.0	3.3±1.9	6.42
$3s_1'''$	3	9.2±2.2	17.2	8.1±2.0	11.4	5.5±1.3	4.80
$3d_4'$	4	34±8	58.2	19±4	31.7	3.4±1.8	4.76

explained in Sec. IV A. Excitation into these $J=2$ levels must involve a ''higher-order'' Coulomb interaction and/or electron exchange. The excitation functions of these levels, however, are rather similar to those of the $J=0$ and $J=4$ levels, which are excited by exchange interaction only. In other words, the higher-order Coulomb interaction appears not to have much influence over the exchange interaction on the shape of the excitation functions of these four levels.

The $J=3$ levels contain the $^1F_3$ singlet component which connects with the ground level through the $k=3$ multipole so that excitation into these levels can proceed via a first-order Coulomb process, in addition to the exchange interaction. The excitation functions of these levels, notably $3d_1'$ and $3s_1'''$, have a broader shape than those of the even-J levels. Of the three $J=3$ levels, the $3d_4$ excitation function is narrower than the other two. This can be explained on the grounds that the $3d_4$ wave function [15] has only 13% singlet ($^1F_3$) character as compared to 43% for $3d_1'$ and 44% for $3s_1'''$. Since the first-order Coulomb process arises from the singlet component of the wave function, the $3d_4$ level is less benefited by the Coulomb process compared to $3d_1'$ and $3s_1'''$, and thus shows more resemblance to spin-changing excitation.

To analyze the magnitude of the cross sections, we turn to Table I, which contains the direct excitation cross sections for the various levels at several different incident electron energies. Note that the $J=3$ levels have generally larger cross sections at higher energy than the even-J levels, in agreement with the general principles discussed in Sec. IV A. For the $3p^5 4p$ levels, we found the opposite to be the case [1]. This reversal occurs because the $3p^5 4p$ and $3p^5 3d$ configurations have opposite parity as explained in Sec. IV A. Excitations into the purely triplet levels ($2s_3$, $2s_5$, $3d_6$, $3d_4'$) are solely due to electron exchange whereas an additional path of higher-order Coulomb process is available for the $3d_1''$, $3d_3$, $3s_1''$, and $3s_1'''{}'$ levels. However, we do not see a discernible difference in the magnitude of the cross sections for these two groups of levels. (Note that these two groups also exhibit very similar excitation functions, as remarked earlier.)

E. The $3p^5 nf$ levels

Optical emission cross sections for the $3p^5 4f \rightarrow 3p^5 3d$ and $3p^5 5f \rightarrow 3p^5 3d$ have been measured for determining the total cascade radiation into the $3p^5 3d$ levels. As it turns out, cascade from the $3p^5 nf$ levels is generally comparable to cascade from $3p^5 np$ except for the case of $3d_6$. A breakdown of the cascade and direct excitation contributions to the apparent cross sections at 40 eV, along with the fractions of the cascades originating from the nf levels, are given in Table II.

Since transitions into the $3p^5 3d$ configuration are the only radiative decay channels of the $3p^5 4f$ levels, our measurements also provide the apparent excitation cross sections for the $3p^5 4f$ levels. Although this paper is mainly concerned with excitation into the $3p^5 3d$ and $3p^5 5s$ levels, we present the $3p^5 4f$ results since no such data have been published in the literature to our knowledge.

For the $3p^5 4f$ configuration, the $4f$ electron interacts weakly with the $3p^5$ because of its nonpenetrating character. The angular momentum vector coupling can be well approximated by the *j-l* scheme in which the angular momentum of the $3p^5$ core, denoted by j, which may be 3/2 or 1/2, is coupled with the orbital angular momentum l of the outer electron to form K, which further couples with the spin of the outer electron, resulting in the total angular momentum J, with $J=K\pm 1/2$ for each K. Combining the lower core-doublet member $j=3/2$ with $l=3$ for the nf electron gives $K=9/2,7/2,5/2$, and 3/2, which are $4V,4U,4Y$, and $4X$, respectively in Paschen's notation. Upon adding the electron spin of the $4f$ electron, each K level is split in two, with $J=K\pm 1/2$, but we do not resolve them in our experiment. The $4V,4U,4Y$, and $4X$ levels span a range of 62 cm^{-1}, which is much smaller than the $^2P_{3/2}-{}^2P_{1/2}$ splitting of the $3p^5$ core (1431 cm^{-1}). We also have another set of levels associated with $j=1/2$ and $l=3$, which are called $4W$ ($K=7/2$) and $4Z$ ($K=5/2$).

The apparent excitation cross sections for the $4V,4U,4Y,4X,4W$, and $4Z$ levels are given in Fig. 5. None of these curves shows a broad peak near 80 eV, as the $3p^5 4f$ configuration is not optically connected to the ground state. Interpretation of these data is complicated by the fact that each curve represents the contribution from the two doublet members ($J=K\pm 1/2$) and that the cross sections include cascades from the higher levels. We note, however, that the $4W$ and $4Z$ curves have lower apparent cross sections than the other $3p^5 4f$ levels, suggesting lower cross sections for the levels associated with the $^2P_{1/2}$ core.

F. Comparison with theoretical cross sections

Bubelev and Grum-Grzhimailo have published the only theoretical calculations of the $3p^5 5s$ and $3p^5 3d$ configurations of which we are aware [17]. Table III compares their results with ours. We find reasonable agreement for the $2s_5$, $3d_1''$, $3s_1''$, and $3s_1'''{}'$ levels, but their $3d_5$ and $3d_3$ cross sections are much larger than ours. Recently, an extensive comparison between theory and experiment for excitation into the $3p^5 4s$ and $3p^5 4p$ levels has been published [18]. The results of the present work on the $3p^5 5s$ and $3p^5 3d$ levels should provide the basis for a more comprehensive study.

ACKNOWLEDGMENTS

The authors wish to thank Michael D. Stewart, Jr. and Dan F. Sullivan, who assisted in the data acquisition work. Thanks are also due to the late Dr. S. Chung for providing us with the intermediate-coupling wave functions, and to Dr. John T. Fons for designing much of the detection system. As always, discussions with Dr. John Boffard have been extremely helpful. This work was supported by the U.S. Air Force Office of Scientific Research.

[1] J. E. Chilton, J. B. Boffard, R. S. Schappe, and C. C. Lin, Phys. Rev. A **57**, 267 (1998).
[2] J. T. Fons and C. C. Lin, Phys. Rev. A **58**, 4603 (1998).
[3] J. E. Chilton and C. C. Lin, Phys. Rev. A **58**, 4572 (1998).
[4] See, for example, J. M. Ajello, G. K. James, B. Franklin, and S. Howell, J. Phys. B **23**, 4355 (1990); J. W. McConkey and F. G. Donaldson, Can. J. Phys. **51**, 914 (1973).
[5] R. S. Schappe, M. B. Schulman, L. W. Anderson, and C. C. Lin, Phys. Rev. A **50**, 444 (1994).
[6] J. K. Ballou, C. C. Lin, and F. E. Fajen, Phys. Rev. A **8**, 1797 (1973).
[7] S. Tsurubuchi, T. Miyazaki, and K. Motohashi, J. Phys. B **29**, 1785 (1996).
[8] A. R. Filippelli, C. C. Lin, L. W. Anderson, and J. W. McConkey, Adv. At., Mol., Opt. Phys. **33**, 1 (1994).
[9] P. R. Griffiths and J. A. de Haseth, *Fourier Transform Infrared Spectrometry* (John Wiley & Sons, New York, 1986).
[10] See, for example, R. M. St. John, F. L. Miller, and C. C. Lin, Phys. Rev. **134**, A888 (1964).
[11] E. M. Purcell, Astrophys. J. **116**, 457 (1952).
[12] J. B. Boffard, G. A. Piech, M. F. Gehrke, L. W. Anderson, and C. C. Lin, Phys. Rev. A **59**, 2749 (1999).
[13] F. A. Sharpton, R. M. St. John, C. C. Lin, and F. E. Fajen, Phys. Rev. A **2**, 1305 (1970).
[14] R. D. Cowan and K. L. Andrew, J. Opt. Soc. Am. **55**, 502 (1965).
[15] S. Chung (private communications).
[16] V. I. Ochkur, Zh. Éksp. Teor. Fiz. **45**, 734 (1963) [Sov. Phys. JETP **18**, 503 (1964)].
[17] V. E. Bubelev and A. N. Grum-Grzhimailo, J. Phys. B **24**, 2183 (1991).
[18] D. H. Madison, C. M. Maloney, and J. B. Wang, J. Phys. B **31**, 873 (1998).